OPTICAL PROPERTIES AND ELECTRONIC STRUCTURE OF POLYCRYSTALLINE Cu-($In_{1-X}Ga_X$)-Se ALLOYS

M. León[a*], S. Levcenko[b], J.M. Merino[a], E.J. Friedrich[a], and E. Arushanov[b]

[a]*Universidad Autónoma de Madrid, Departamento Física Aplicada, C-XII, 28049, Madrid, Spain*
[b]*Institute of Applied Physics, Academy of Sciences of Moldova, 5, Academiei str., MD-2028, Chisinau, Republic of Moldova*
*****E-mail: maximo.leon@uam.es*
(Received 23 September 2008)

Abstract

The optical properties of bulk Cu-($In_{1-x}Ga_x$)-Se alloys grown by the Bridgman method are presented. The optical measurements were performed at room temperature in the photon energy range from 0.8 to 4.7eV using a variable-angle spectroscopic ellipsometer. The spectral dependences of the complex dielectric function, the refractive index, the absorption coefficient and the normal-incidence reflectivity were derived. The observed structures attributed to the interband transitions E_0, E_{1A}, and E_{1B} were modelled using a modification of the Adachi's model. The model parameters were determined using the simulated annealing (SA) algorithm. The values of E_0 and E_{1A} were found to increase linearly with Ga content.

1. Introduction

$CuInSe_2$ and related chalcopyrite-type semiconductors are leading candidates for absorbers in high-efficiency heterojunction solar cells. Devices based on $CuIn_{1-x}Ga_xSe_2$ have demonstrated efficiencies up to 19.3% [1]. Recent studies have shown the existence of an In-rich n-type material surface layer of $Cu(In_{1-x}Ga_x)_3Se_5$ on the absorber in some high efficiency thin-film cells. This layer, identified as an ordered defect compound (ODC) is expected to play an important role in the performance of the high-efficiency $CuIn_{1-x}Ga_xSe_2$–based solar cells [2, 3]. In a recent report of surface properties of $CuGaSe_2$ thin films, evidences of band gap widening [4] together with deviations from stoichiometry pointing to formation of ODC-related phases were also shown [5]. Therefore, a detailed study of the physical properties of these ODCs is important. However, the characteristics of ODC have not been yet well determined. Some optical measurements were carried out on $Cu_2In_4Se_7$ (I247), $CuGa_3Se_5$ (G35), and $CuGa_5Se_8$ (G58) thin films and bulk samples and values of the fundamental band gap E_g were estimated [6-15]. Only absorption coefficients were determined for $Cu(In_{1-x}Ga_x)_3Se_5$ [16, 17] and $Cu(In_{1-x}Ga_x)_2Se_{3.5}$ [18] thin-film alloys by optical transmission data and the band gap values E_g were estimated. More recently the ellipsometric spectra of several $Cu(In_{1-x}Ga_x)_3Se_5$ polycrystalline alloys have been published [19]. Spectroscopic ellipsometry (SE) is an excellent technique to investigate the optical response of semiconductors, in particular, for determining the complex dielectric function $\varepsilon(\omega) = \varepsilon_1(\omega) + i\varepsilon_2(\omega)$. Accurate knowledge of the dielectric function over a wide range of wavelengths is indispensable for many applications [20]. In this work the optical properties of six Cu-($In_{1-x}Ga_x$)-Se alloys grown by the Bridgman method are presented. The optical measurements were performed at

room temperature in the photon energy range from 0.8 to 4.7eV, at two incidence angles, 60° and 70°, using a variable-angle spectroscopic ellipsometer. A two-phase model (atmosphere-sample) was used to analyze the ellipsometry spectra. The spectral dependence of the complex dielectric functions was derived. The observed structure attributed to the interband transitions E_0, E_{1A}, and E_{1B} have been modelled using a modification of the Adachi's model. The model parameters, including the energies corresponding to the lowest direct gap and higher critical-points, have been determined using the simulated annealing (SA) algorithm. The dependence on composition of E_0 and E_{1A} as a function of Ga content has been obtained.

2. Theoretical model

The Adachi's model has been successfully applied to model the dielectric function as well as the optical constants of III-V and I-III-VI_2 compounds [21-23]. The complex dielectric function as a function of energy $E = \hbar\omega$ is described by the sum of terms corresponding to one-electron contributions at critical points $E_{0\alpha}$ ($\alpha = A, B, C$) and $E_{1\beta}$ ($\beta = A, B$), $\varepsilon_0(E)$ and $\varepsilon_1(E)$ respectively, plus an additive constant a

$$\varepsilon(E) = \varepsilon_0(E) + \varepsilon_1(E) + a. \tag{1}$$

The $E_{0\alpha}$ ($\alpha = A, B$, and C) transition in chalcopyrite crystals is assigned to the three-dimensional (3D) M_0 critical point. Assuming that the valence and conduction bands are parabolic and using the Kramers–Kronig transformation, the contribution of this transition to $\varepsilon_0(E)$ can be written as

$$\varepsilon_0(E) = \sum_{\alpha=A,B,C} A_{0\alpha} E_{0\alpha}^{-3/2} f(\chi_{0\alpha}), \text{ with}$$
$$A_{0\alpha} = (4/3)(3/2\mu_{0\alpha})^{3/2} P_{0\alpha}^{\ 2}, \; f(\chi_{0\alpha}) = \chi_{0\alpha}^{-2}[2-(1+\chi_{0\alpha})^{1/2}-(1-\chi_{0\alpha})^{1/2}], \tag{2}$$
$$\chi_{0\alpha} = (E + i\Gamma)/E_{0\alpha}$$

In Eq. 2 $\mu_{0\alpha}$ is the combined density-of-states mass, $P^2_{0\alpha}$ is the squared momentum-matrix element, and Γ is the damping energy of the $E_{0\alpha}$ transition. It is worth mentioning that normally one should calculate the separate contributions from $E_{0\alpha}$ ($\alpha = A$, B, and C) critical points according to Eq.2, but in our case, splitting among these critical points is not observed, and $E_{0\alpha}$ has been treated as a single degenerate one. Contributions of the two-dimensional (2D) M_0 critical points $E_{1\beta}$ are given in the Adachi's model [22] by

$$\varepsilon_1(E) = -\sum_{\beta=A,B} B_{1\beta}\chi_{1\beta}^{-2} Ln(1-\chi_{1\beta}^{\ 2}), \text{ with}$$
$$\chi_{1\beta} = (E + i\Gamma_{1\beta})/E_{1\beta}, \tag{3}$$

where $B_{1\beta}$ and $\Gamma_{1\beta}$ are the strengths and damping constants of the $E_{1\beta}$ transitions, respectively.

Djurisic [23] et al. have proposed the acceptance-probability-controlled simulated annealing (APCSA) algorithm to obtain the model parameters. It is known that all fitting routines based on classical optimization algorithms, like Levenberg–Marqardt or simplex algorithms, require initial parameter values close to the final ones to provide a meaningful solution and it is usually hard to provide good initial values for adjustable parameters of the model. Therefore, to determine accurately the model parameters, one should employ a global optimization routine, such as a simulated annealing algorithm employed in [24]. In this work, the model parameters were determined using the APCSA algorithm through minimizing the following objective function:

$$F = \sum_{i=1}^{N} \left(\left| \frac{\varepsilon_1(E_i)}{\varepsilon_1^{\,\text{expt}}(E_i)} - 1 \right| + \left| \frac{\varepsilon_2(E_i)}{\varepsilon_2^{\,\text{expt}}(E_i)} - 1 \right| \right)^2, \tag{4}$$

where the summation is performed over the available experimental points, and $\varepsilon_1^{expt}(E_i)$, $\varepsilon_1(E_i)$ $\varepsilon_2^{expt}(E_i)$, $\varepsilon_2(E_i)$ are, respectively, the experimental and calculated values of the real and imaginary parts of complex dielectric function at point E_i.

3. Experimental methods

The $Cu(In_{1-x}Ga_x)_3Se_5$ crystals were synthesized from the individual elements with 99.9999% purity in a vacuum sealed quartz tube. This ampoule was introduced in a rocking horizontal furnace that was gently heated to 1100ºC, avoiding overpressures, and cooled slowly, 5-10ºC/h. The energy dispersive X-ray microanalysis (EDAX) was used to measure the composition of the samples. The results of such analysis have been gathered in Table 1.

Table 1. Compositional data of samples obtained by energy dispersive X- ray microanalysis (EDAX).

Samples	Cu at %	In at %	Ga at %	Se at %	(In+Ga)/Cu	Se/Cu
$Cu_2In_4Se_7$ (I247)	16.6	31.1		52.3	1.9	3.1
$CuIn_3Se_5$ (I35S)	11.2	30.9		57.9	2.76	5.17
Cu $(In_{0.58}Ga_{0.41})_2Se_{3.2}$ (IG1)	16.2	18.5	13.2	52.1	1.96	3.22
Cu $(In_{0.33}Ga_{0.69})_3Se_{4.8}$ (IG3)	11.3	11.3	23.3	54.1	3.06	4.79
$Cu_{1.2}(In_{0.61}Ga_{0.39})_3Se_{4.8}$ (IG2)	13.3	20.3	12.7	53.7	2.48	4.04
$CuGa_3Se_5$ (G35B)	13.1		34.5	52.4	2.63	4.0

The structural analysis was performed by X-ray diffraction and it was found that the ingots were polycrystalline single phase, presenting tetragonal structures, as is shown in Fig. 1. According to References [17] and [18], the values of E_g are practically the same for $Cu(In_{1-x}Ga_x)_2Se_{3.5}$ and $Cu(In_{1-x}Ga_x)_3Se_5$ solid solutions, with a negligible dependence on the Cu and Se contents. This fact permitted us to analyze IG1 as a sample with properties similar to those of a film with the composition $Cu_{1.5}(In_{0.58}Ga_{0.41})_3Se_{4.8}$. In the following, the analysis has been performed considering all samples belonging to the $Cu(In_{1-x}Ga_x)_3Se_5$ solid solution, and the results have been analyzed as a function of the Ga content.

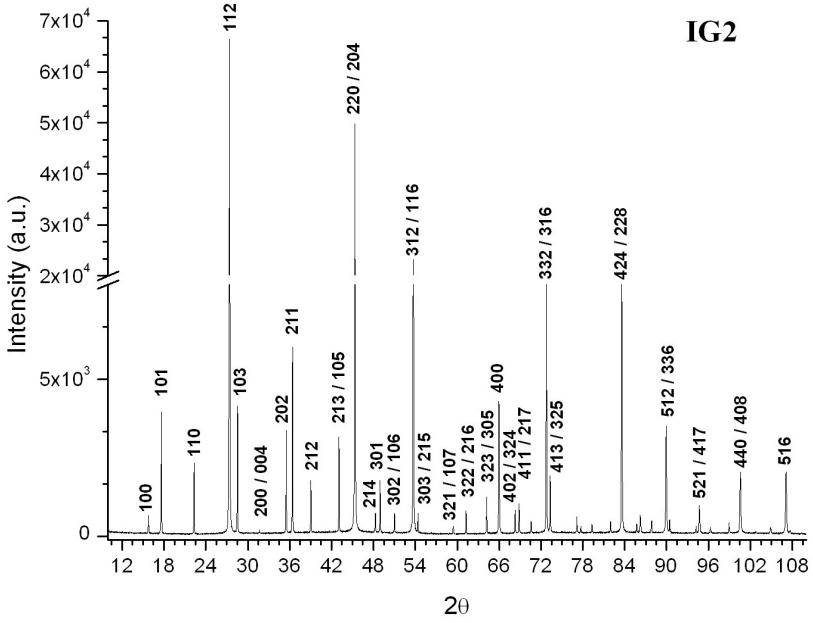

Fig. 1. X ray powder diffraction diagram of IG2 sample. The indexing is depicted for all reflections below 2θ=70º, for higher 2θ values most of indexing is omitted for clarity.

The optical measurements were performed with a variable-angle spectroscopic ellipsometer at room temperature, in the photon energy range from 0.8 to 4.7 eV, at two incidence angles, Φ=60° and Φ=70° [25]. In order to remove undesired over layers formed on the surface, the samples were specially prepared as described in Ref. [26]; hence, a two-phase model (atmosphere-sample) was used to analyze the ellipsometry spectra [26, 27]. The complex dielectric functions have been determined following equation 1 of Ref. [28]. The features observed in the complex dielectric function spectra $\varepsilon = \varepsilon(\hbar\omega)$ have been described in terms of the interband transitions, using the previously explained Adachi's model.

4. Results and discussions

The experimental pseudodielectric functions, $\varepsilon(\omega) = \varepsilon_1(\omega) + i\varepsilon_2(\omega)$, of the samples I35S, IG1, IG2, IG3, and G35B are presented in Fig. 2. The line shapes of $\varepsilon_1(\omega)$ and, $\varepsilon_2(\omega)$ in all our samples are dominated by two distinct peaks. In the spectral range under consideration, the line shape of the dielectric function is determined by the electronic band structure and the observed structures usually correspond to transitions at high–symmetry points or lines in the Brillouin zone. These CPs are characterized by a high joint density of states combined with nonvanishing transition matrix elements. The dielectric function is considered as a sum of the contributions from all allowed transitions at CPs.

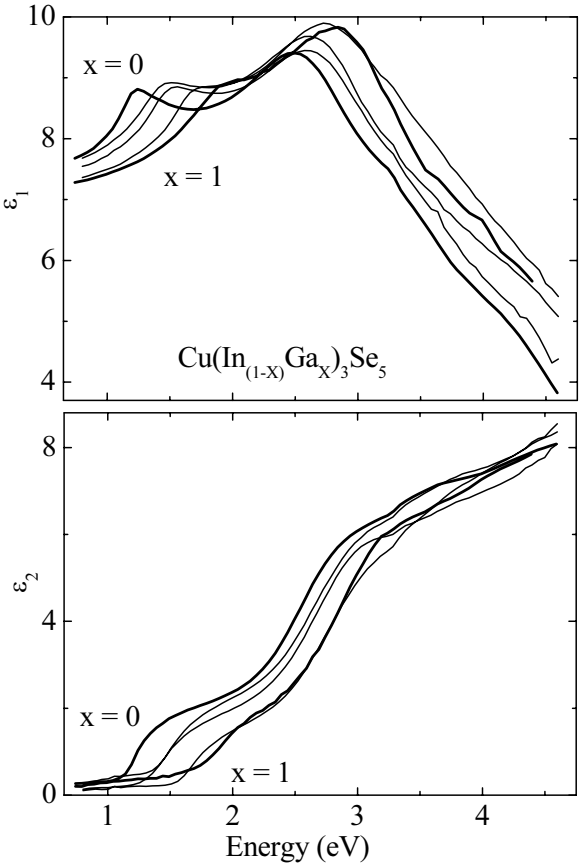

Fig. 2. Real ε_1 and imaginary ε_2 parts of the dielectric function vs. energy for $Cu(In_{1-x}Ga_x)_3Se_5$ alloys, I35S, IG1, IG2, IG3, and G35B samples. The spectra corresponding to the ternary end compounds are plotted with thicker lines (I35S and G35B).

The Adachi's model was applied to calculate the dielectric function as well as the optical constants of the studied crystals. The resulting analytical lines in Fig. 3 have been obtained from the fits of the experimental data considering *3D*-type CPs in the lowest energy region, E_0, and *2D* type in the intermediate and high energy region, E_1. The *A, B, E* and *Γ* model parameters calculated using the SA algorithm are given in Table 2. The lowest *E* value observed in the region below 1.7 eV

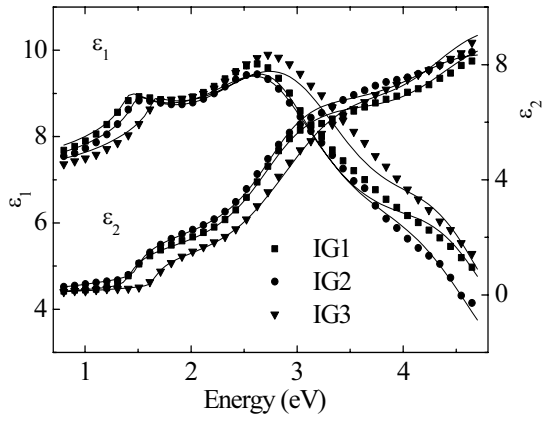

Fig. 3. Real ε_1 and imaginary ε_2 parts of the dielectric function vs. energy for IG1, IG2, and IG3 samples. Solid squares, circles and triangles represent the experimental data, while the solid lines correspond to the theoretical fits.

corresponds to the fundamental energy gap value, $E_0 = E_g$, well distinguished for each studied sample (Figs. 2, 3). In addition, a second, E_{1A}, and a third, E_{1B}, energy threshold appear in the region 2.5-4.5 eV (Table 2).

An excellent agreement between our calculations and the experimental data on $\varepsilon_1^{expt}(\omega)$ and $\varepsilon_2^{expt}(\omega)$ has been observed for all studied samples. The fit with the adjustable parameters given in Table 2 is shown in Fig. 3.

Table 2. Model parameter values.

Parameters	Samples					
	I247	I35S	IG1	IG2	IG3	G35B
$A(eV^{1.5})$	5.15	4.20	5.89	6.02	5.98	7.40
$E_0(eV)$	1.125	1.18	1.40	1.47	1.64	1.85
$\Gamma(eV)$	0.03	0.005	0.038	0.031	0.019	0.043
$B_{1A}(eV)$	2.38	2.95	2.69	3.11	2.60	2.48
$E_{1A}(eV)$	2.55	2.63	2.73	2.77	2.90	2.90
$\Gamma_{1A}(eV)$	0.31	0.41	0.40	0.43	0.42	0.32
α	0.88	0.03	0.12	-	0.20	0.25
$B_{1B}(eV)$	3.28	3.92	3.97	3.50	3.99	3.7
$E_{1B}(eV)$	4.01	4.13	4.43	4.22	4.39	4.24
$\Gamma_{1B}(eV)$	0.73	0.87	0.69	0.749	0.64	0.73

Band structure calculations are not available for $Cu(In_{1-x}Ga_x)_3Se_5$; however, the structure of the fundamental absorption edge of chalcopyrites is well understood [29]. These crystals are semiconductors with a direct fundamental gap at the Brillouin-zone center, Γ. Based on the band-structure calculations from Jaffe and Zunger [30] for the ternary end compounds and relating the observed transitions to those of the binary zinc-blend analogues, the main transitions that contribute to $\varepsilon(\omega)$ could be assigned to critical points at the Brillouin-zone center, Γ, and edge points, N and T. The labelling of these transitions is described in Ref. [31], and is related to the standard zinc-blend notation.

The band structure calculations obtained for $CuInSe_2$ (CIS) and $CuGaSe_2$ (CGS) [20, 21] have also been used to identify the energy values observed in $Cu(In_{1-x}Ga_x)_3Se_5$. The energy threshold of the fundamental absorption edge, $E_0 = E_g$, well identified in the spectra of studied materials (Figs. 2, 3), can be related to an electronic transition at the Γ point. The estimated values of E_g at room temperature, 1.47 eV (x = 0.39), 1.4 eV (x = 0.41), and 1.64 eV (x = 0.69) for the samples belonging to the $Cu(In_{1-x}Ga_x)_3Se_5$ solid solution are in the range between those previously determined for the two ternary end compounds, $CuIn_3Se_5$ [28] and $CuGa_3Se_5$ [25, 32]. In addition, these values are in an excellent agreement with those reported for $Cu(In_{1-x}Ga_x)_3Se_5$ [17] and $Cu(In_{1-x}Ga_x)_2Se_{3.5}$ [18] films with the same content on Ga (value of x), as is shown in Fig. 4.

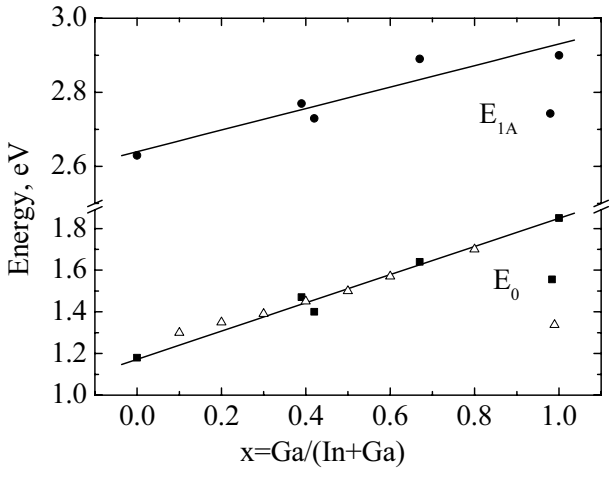

Fig. 4. Compositional dependence of the E_0 and E_1 (A) in $Cu(In_{1-x}Ga_x)_3Se_5$ alloys. Solid squares and circles represent data after this work, while open triangles correspond to data after Negami et al. [17].

In the region between 2.5 and 4.5 eV, two transitions, named as E_{1A} and E_{1B}, have also been observed. We have assumed that they can be related to *N*- type transitions after references 26 and 31, where ellipsometric data for CIS and CGS compounds were analyzed. The measured energy separation between these two transitions corresponds to the crystal-field splitting of the valence band at the *N* point in the Brillouin-zone. In the present work, the crystal-field splitting at the *N* point was found to lie between 1.5 - 1.7 eV, close to that (1.3 - 1.5 eV) estimated for $CuGa_3Se_5$ [25, 32] and $CuIn_3Se_5$ [28].

As it can be observed in Fig. 4, our results indicate a linearity in the compositional dependence of E_0 and E_{1A}, as well as some scattering in the E_{1B} values laying around 4.30 ± 0.15 eV, from Table 2. The exact character of the variation of E_{1B} vs. the Ga content cannot be easily determined because such variation is quite small (about ± 4%) and the accuracy in the determination of the E_{1B} value is not high enough.

Optical parameters, namely, the complex refractive index $n^*=n+ik$, normal-incidence reflectivity *R* and the absorption coefficient α, can be obtained from the present study in the form of practical functions, since they are directly related to the complex dielectric function $\varepsilon(E) = \varepsilon_1(E) + i\varepsilon_2(E)$.

The real refractive index *n* and the extinction coefficient *k* are given by

$$n(E) = \left(\frac{\left[\varepsilon_1(E)^2 + \varepsilon_2(E)^2\right]^{1/2} + \varepsilon_1(E)}{2} \right)^{1/2} \tag{5}$$

$$k(E) = \left(\frac{\left[\varepsilon_1(E)^2 + \varepsilon_2(E)^2\right]^{1/2} - \varepsilon_1(E)}{2} \right)^{1/2} \tag{6}$$

The absorption coefficient α and the normal-incidence reflectivity *R* can be written as

$$\alpha(E) = \frac{4\pi}{\lambda} k(E) \tag{7}$$

$$R(E) = \frac{\left[n(E)-1\right]^2 + k(E)^2}{\left[n(E)+1\right]^2 + k(E)^2} \tag{8}$$

where λ is the wavelength of light in the vacuum.

The spectral dependences of α, *R,* the refractive index *n,* and the extinction coefficient *k* from the experimental data, as well as the ones calculated using the Adachi's model and the SA algorithm, for the three intermediate samples are plotted in Figs. 5 and 6.

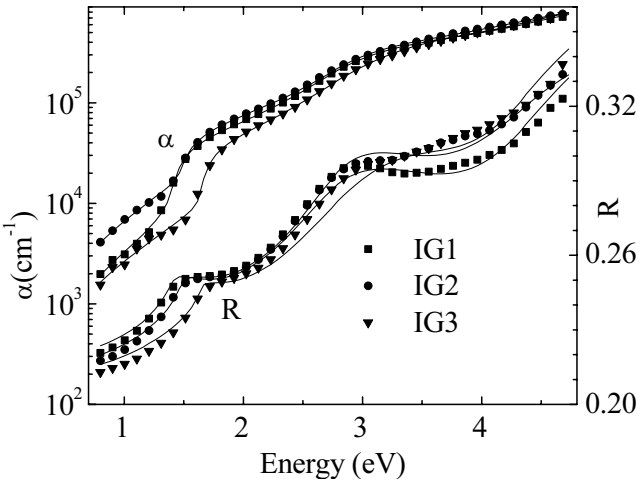

Fig. 5. Spectral dependences of the absorption coefficient, α, and the normal-incidence reflectivity, R, for IG1, IG2 and IG3 samples: experimental (solid squares, circles, and triangles) and theoretically calculated using the Adachi's model and the SA algorithm (solid lines).

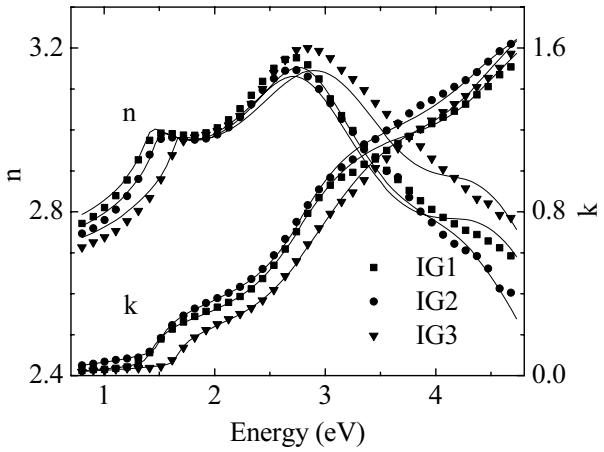

Fig. 6. Spectral dependences of the real refraction index, n, and the extinction coefficient, k for IG1, IG2 and IG3 samples: experimental (solid squares, circles, and triangles) and theoretically calculated using the Adachi's model and the SA algorithm (solid lines).

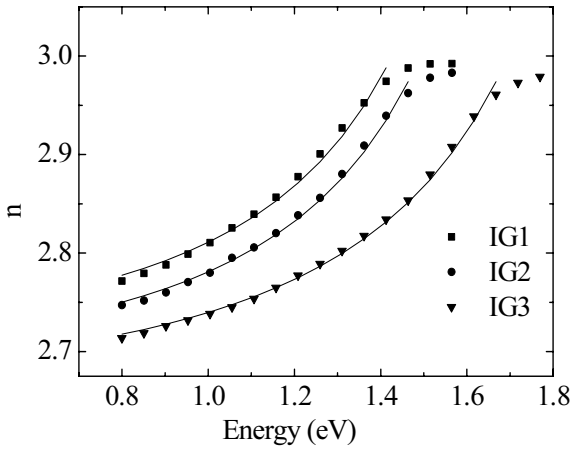

Fig. 7. Real refractive index n vs. photon energy for IG1, IG2, and IG3 samples. The solid line shows the calculated result after Eq. 9. Solid squares, circles, and triangles represent the experimental data.

A good agreement is observed for all the studied samples and the obtained values of the interband CP parameters (strength, threshold energy, and broadening) given in Table 2. All these optical spectra were found to reveal distinct structures at these points.

The experimental data of the refractive index *n* have also been analyzed in the non-absorbing region using a simple theoretical model, namely the first-order Sellmeier's equation [22, 25, 28]

$$n^2(\lambda) = A + \frac{\lambda^2}{\lambda^2 - B} \tag{9}$$

where *A* and *B* are the fitting parameters. The solid line in Fig. 7 represents the fitting of Eq. (9) to the experimental data for the intermediate samples. The values of the fitting parameters *A* and *B* for all samples are gathered in Table 3, both values increase with the content on In.

Table 3. Sellmeier's equation fitting parameters and high-frequency dielectric constant values.

Parameters	Samples					
	I247	I35S	IG1	IG2	IG3	G35B
A	6.6	6.38	6.48	6.34	6.22	6.23
B	0.61	0.63	0.46	0.43	0.34	0.29
ε_∞	7.7	7.38	7.48	7.34	7.22	7.23

As $\lambda \to \infty$, the electronic contribution to the dielectric function approaches the limiting value ε_∞**,** i. e., the high-frequency dielectric constant**.** The value of $\varepsilon_\infty = n^2\ (\lambda \to \infty) = A+1$ behave as *A*, increasing with the content on In.

5. Conclusions

The optical properties of several $Cu(In_{1-x}Ga_x)_3Se_5$ samples have been studied by spectroscopic ellipsometry. The spectral dependence of the real and imaginary parts of the complex dielectric function, as well as of the complex refractive index, extinction and absorption

coefficients, and the normal-incidence reflectivity for several $Cu(In_{1-x}Ga_x)_3Se_5$ samples with x in the 0-1 range are modelled in the 0.8-4.7 eV photon energy range using a modification of Adachi´s model for the complex dielectric function of semiconductors and the SA algorithm. An excellent agreement with the experimental data is obtained and the model parameters (strength, threshold energy, and broadening) have been determined. Both spectral dependences of the optical functions and the critical point analysis are expected to be useful in studies of solar cells and other heterostructures that contain these materials. It has been shown that both the fundamental gap E_g and E_{1A} values increase linearly with the Ga content. In addition, the high-frequency dielectric constant, ε_∞, increases with the In content of sample.

Acknowledgements

Financial support from Comunidad de Madrid (Project FOTOFLEX S-0505/ENE/0123) is acknowledged. One of us (SL) would like to thank CRDF-MRDA (project #MYSSP-1402) for financial support.

References

[1] K. Ramanathan, G. Teeter, J. Keane, and R. Noufi, Thin Solid Films, 480-481, 499, (2005).
[2] J. Kessler, D. Schmid, R. Schafler, H.W. Schock, and S. Menezes, Proc. 23rd IEEE Photovoltaic Conference, Louisville, New York: IEEE, 549, (1993).
[3] H.Z. Xiao, L. Yang Chung, and A. Rockett, J. Appl. Phys., 76, 1503, (1994).
[4] A. Meeder, L. Weinhardt, R. Stresing, D. Fuertes Marrón, R. Würz, S.M. Babu, Th. Schedel-Niedrig, M.Ch. Lux-Steiner, S. Heske, and E. Umbach, J. Phys. Chem. Solids, 64, 1553, (2003).
[5] R. Würz, M. Rusu, Th. Schedel-Niedrig, M.Ch. Lux-Steiner, H. Blum, M. Hävecker, E. Kleimenov, A. Knop-Gericke, and R. Schlogl, Surf. Science, 64, 1553, (2005); S. Lehmann, M. Bär, D. Fuertes Marrón, P. Pistor, S. Wiesner, M. Rusu, I. Kötschau, I. Lauermann, A. Grimm, S. Sokoll, Ch.-H. Fischer, Th. Schedel-Niedrig, M. Ch. Lux-Steiner, and Ch. Jung, Thin Sol. Films, 511-512, 623, (2006).
[6] Y.B.K. Reddy and V.S. Raja, Materials Letters, 58, 1839, (2004).
[7] C. Rincon, S.M. Wasim, G. Marin, and G. Sanchez Perez, J. Appl. Phys., 93, 8939, (2003).
[8] Takayuki Negami, Naoki Kohara, Mikihiko Nishitani, Takahiro Wada, and Takashi Hirao, Appl. Phys. Lett., 67, 825, (1995).
[9] S. Mahanty, J.M. Merino, R. Diaz, F. Rueda, J.L. Martin de Vidales, and M. Leon, Inst. Phys. Conf. Ser.,152, 499, (1998).
[10] G. Marin, C. Rincon, S.M. Wasim, G. Sanches Perez, and I. Molina, J. Alloys Compounds, 283, 1, (1999).
[11] S. Shirakata, S. Chichubu, H. Miyake, S. Isomura, H. Nakanishi, and K. Sugiyama, Inst. Phys. Conf. Ser., 152, 598, (1998).
[12] S.M. Wasim, G. Marin, C. Rincon, P. Bocaranda, and G. Sanchez Perez, J. Phys. Chem. Sol., 61, 669, (2000).
[13] C. Rincon, S.M. Wasim, G. Marin, and I. Molina, J. Appl. Phys., 93, 780, (2003).
[14] G. Marin, S.M. Wasim, C. Rincon, G. Sanches Perez, P. Bocaranda, I. Molina, R. Guevara, and J.M. Delgado, J. Appl. Phys., 98, 8280, (2004); L. Duran, C. Guerrero, E. Hernandes, J.M. Delgado, J. Contreras, S.M. Wasim, and C.A. Durante Rincon, J. Phys. Chem. Solids, 64, 1907, (2003).
[15] N.S. Orlova, I.V. Bodnar, and T.L. Kushner, J. Phys. Chem. Sol., 64, 1895, (2003).

[16] G. Marín, S. Tauleigne, S.M. Wasim, R. Guevara, J.M. Delgado, C. Rincón, A.E. Mora, and G. Sánches Pérez, Mat. Res. Bull., 33, 1057, (1998).
[17] T. Negami, N. Kohara, M. Nishitani, T. Wada, and T. Hirao, Appl. Phys. Lett., 67, 825, (1995).
[18] T. Tanaka, N. Tanahashi, T. Yamaguchi, and A.Yoshida, Sol. Energy Mater. Sol. Cells 50, 13 (1998).
[19] M. León, R. Serna, S. Levcenko, G. Gurieva, J.M. Merino, E.J. Friedrich, and E. Arushanov, J. Appl. Phys., 104, 093507, (2008).
[20] P. Lautenschlager, M. Garriga, S. Logothetidis, and M. Cardona, Phys. Rev. B, 35, 9174, (1987); M. Cardona, Modulation spectroscopy, Academic, New York, 344, 1969.
[21] T. Kawashima, S. Adachi, H. Miyake, and K. Sugiyama, J. Appl. Phys. 84, 5202, (1998).
[22] T. Kawashima, H. Yoshikawa, S. Adachi, S. Fuke, and K. Ohtsuka, J. Appl. Phys., 82, 3528, (1997).
[23] A.B. Djurisic, A.D. Rakic, and J.M. Elazar, Phys. Rev. E, 55, 4797, (1997).
[24] A. Corana, M. Marchesi, C. Martini, and S. Ridella, ACM T. Math. Software, 13, 262, (1987).
[25] M. León, R. Serna, S. Levcenko, A. Nateprov, A. Nicorici, J.M. Merino, and E. Arushanov, J. Appl. Phys., 101, 013524, (2007).
[26] M.I. Alonso, M. Garrida, C.A. Durante Rincon, and M. Leon, J. Appl. Phys., 88, 5796, (2000); J.G. Albornoz, R. Serna, and M. León, J. Appl. Phys., 97, 103515, (2006).
[27] R.M.A. Azzam and N.M. Bashara, Ellipsometry and Polarized Light, 1st ed., North-Holland, Amsterdam, 282, 1977.
[28] M. León, R. Serna, S. Levcenko, A. Nicorici, J.M. Merino, E.J. Friedrich, and E. Arushanov, J. Appl. Phys., 103, 103503, (2008).
[29] J.L. Shay and J.H. Wernick, Ternary Chalcopyrite Semiconductors: Growth, Electronic Properties, and Applications. Pergamon, Oxford, 236, 1975.
[30] E. Jaffe and A. Zunger, Phys. Rev. B, 28, 5822, (1983).
[31] M.I. Alonso, K. Wakita, J. Pascual, M. Garriga, and N. Yamamoto, Phys. Rev. B, 63, 075203, (2001).
[32] M. León, S. Levcenko, A. Nateprov, A. Nicorici, M. Merino, R. Serna, and E. Arushanov, J. Phys. D, 40, 740, (2007); M. León, S. Levcenko, A. Nateprov, A. Nicorici, J.M. Merino, E.J. Friedrich, R. Serna, and E. Arushanov, J. Appl. Phys., 102, 113503, (2007).